Lecture notes on topological insulators

Ming-Che Chang

Department of Physics, National Taiwan Normal University, Taipei 11677, Taiwan

(Dated: March 28, 2017)

I. WEYL SEMIMETAL

There are two important types of nodal points in 3D. One is the point degeneracy between two energy levels, the other is the point degeneracy between four energy levels, see Fig. 1. To distinguish between them, from now on we call the former a **Weyl point**, and the latter a **Dirac point**. In this chapter, we *only* study the Weyl points.

A. Classification of Weyl node

The Hamiltonian near a Weyl point can be written as

$$\mathsf{H} = \mathbf{d}(\mathbf{k}) \cdot \boldsymbol{\sigma}, \tag{1.1}$$

where $\mathbf{k}$ is the momentum away from the node. If the components of $\mathbf{d}$ are all linear in $\mathbf{k}$, then we call it as a **linear Weyl node**. If at least one of the components of $\mathbf{d}$ is quadratic in $\mathbf{k}$, then we call it as a **quadratic Weyl node**, and so on.

The **topological charge** (or Berry index) of a node is given by the first Chern number (see Sec. **??**),

$$Q_T = \frac{1}{2\pi}\int_{S^2_{\mathbf{k}}} d^2\mathbf{a}\cdot\mathbf{F}, \tag{1.2}$$

$$F_k = \frac{1}{2d^3}\mathbf{d}\cdot\frac{\partial\mathbf{d}}{\partial k_i}\times\frac{\partial\mathbf{d}}{\partial k_j}. \tag{1.3}$$

The integral is over a constant-energy surface with fixed $|\mathbf{d}|$, and i, j, k are in cyclic order. We learned in Sec **??** that the integrand is just (half of) the solid angle of the image $f : S^2_{\mathbf{k}} \to S^2_{\mathbf{d}}$, thus Q_T is the winding number of the map .

For example, given

$$\mathsf{H} = \pm\mathbf{k}\cdot\boldsymbol{\sigma}, \tag{1.4}$$

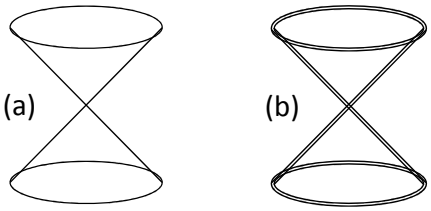

FIG. 1 (a) A Weyl point between two levels. (b) A Dirac point between 2 double-degenerate levels.

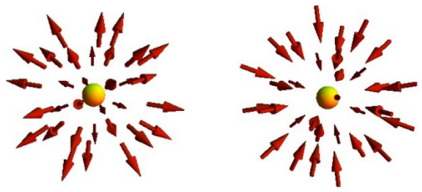

FIG. 2 The textures of $\mathbf{d}(\mathbf{k})$ of two Weyl points with opposite helicities. The figures are from somewhere on the web.

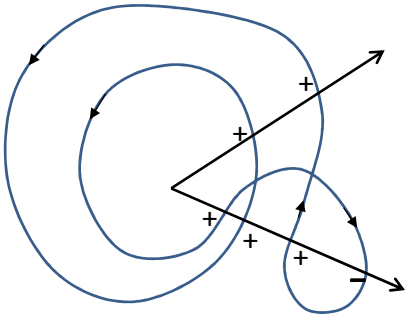

FIG. 3 The winding number is determined by the degree of the map, which is the same irrespective of the direction one peeps.

the textures of $\mathbf{d}(\mathbf{k}) = \pm\mathbf{k}$ around the nodal point are shown in Fig. 2. It is obvious that the winding numbers, and hence the topological charges, are ±1. The sign $\pm$ is called as the **helicity** (or **chirality**) of the Weyl point.

For a general linear node, its topological charge can be obtained simply as the sign of the Jacobian,

$$Q_T = \mathrm{sgn}\left|\frac{\partial d_i}{\partial k_j}\right|, \tag{1.5}$$

which is the same for every point $\mathbf{k}$. The sign simply shows that whether the map preserves or reverses the orientation.

For a Weyl node with higher order, its topological charge can also be determined by the energy dispersion near the node. This is explained below (see the App. of Chang and Yang, 2015) : An image point $\mathbf{d}^r$ is called a **regular point** if the Jacobian $|\partial d^r_i/\partial k_j| \neq 0$. A regular point can have none, or several pre-image points $\mathbf{k}^{(\ell)}$, $\mathbf{d}(\mathbf{k}^{(\ell)}) = \mathbf{d}^r, \ell = 1, \cdots, N$. The degree of the map f is defined as,

$$\deg f = \sum_{\ell=1}^{N} \mathrm{sgn}\left(\left|\frac{\partial d_i}{\partial k_j}\right|_{\mathbf{k}=\mathbf{k}^{(\ell)}}\right). \tag{1.6}$$

It is equal to the winding number, and thus the topological charge $Q_T = \deg f$. **Brouwer's lemma** guarantees that $\deg f$ is the same for every regular points (see Fig. 3). Therefore, one can choose a convenient $\mathbf{d}^r$ to calculate it. For more details, one can see Sec. 10.7 of Felsager, 1998, and Milnor, 1965.

For example, for the following quadratic Weyl node,

$$\mathbf{d}(\mathbf{k}) \simeq \left(\frac{k_y^2}{2} - \frac{k_x^2}{2}, k_x k_y, \pm k_z \right), \tag{1.7}$$

the Jacobian is

$$\left| \frac{\partial d_i}{\partial k_j} \right| = \mp (k_x^2 + k_y^2). \tag{1.8}$$

Choosing $\mathbf{d}_0 = (1/2, 0, 0)$, then there are two pre-images, $\mathbf{k}^{(1)} = (0, 1, 0)$ and $\mathbf{k}^{(2)} = (0, -1, 0)$. They contribute to $Q_T = \mp 2$ in total. A node with $|Q_T| = 2$ is sometimes called as a **double Weyl node**.

If $d_x(\mathbf{k})$ is changed to $(k_x^2 + k_y^2)/2$, then the topological charge would be 0. That is, not all quadratic Weyl nodes are double Weyl nodes.

B. Linear Weyl node

In the following, we focus only on the linear Weyl node. Its gauge structure is similar to that of a magnetic monopole. For example, for the nodal point in Eq. (1.4), the Berry curvature is

$$\mathbf{F} = \mp \frac{1}{2} \frac{\hat{\mathbf{k}}}{k^2}, \tag{1.9}$$

which is the same as the magnetic field of a monopole. (Cf: Berry curvatures of various 2D systems in Sec. **??**.)

Once a Weyl node exists, it is stable against perturbations. Consider

$$H = \pm v \mathbf{k} \cdot \boldsymbol{\sigma} + H', \tag{1.10}$$

H' is an arbitrary perturbation that can be expanded by Pauli matrices,

$$H' = a(\mathbf{k}) + \mathbf{b}(\mathbf{k}) \cdot \boldsymbol{\sigma} \tag{1.11}$$

$$= a(\mathbf{k}) + \mathbf{b}(0) \cdot \boldsymbol{\sigma} + \boldsymbol{\sigma} \cdot \sum_j \left. \frac{\partial \mathbf{b}}{\partial k_j} \right|_0 k_j + O(k^2). \tag{1.12}$$

It's obvious that the second term shifts the position of the node, the third renormalizes the velocity of the Weyl electron, but no gap is opened. That is, the Weyl point remains intact under an arbitrary perturbation. It could disappear only by merging with another node with opposite topological charge.

TABLE I Counting Weyl nodes

time-rev symm	space-inv symm	min number
no	no	2
yes	no	4
no	yes	2
yes	yes	unstable

1. Multiplet of nodes due to symmetry

First, in the absence of space or time symmetry, massless lattice fermions are required to come in pairs with opposite helicities. This is the **Nielsen-Ninomiya theorem** (Nielsen and Ninomiya, 1981a,b), or **fermion-doubling theorem** (see App. **??**). We now consider one of the node with helicity + or −,

$$\mathsf{H} = \pm v \boldsymbol{\sigma} \cdot (\mathbf{k} - \mathbf{k}_0). \tag{1.13}$$

Under time reversal transformation (*if* the pseudo-spin behaves like a spin),

$$\mathbf{k} \to -\mathbf{k}, \quad \boldsymbol{\sigma} \to -\boldsymbol{\sigma}. \tag{1.14}$$

So

$$\mathsf{H} \to \mathsf{H}' = \pm v \boldsymbol{\sigma} \cdot (\mathbf{k} + \mathbf{k}_0). \tag{1.15}$$

Therefore, if there is TRS, then there must be another nodal point at $-\mathbf{k}_0$ with the same helicity.

Under space inversion transformation,

$$\mathbf{k} \to -\mathbf{k}, \quad \boldsymbol{\sigma} \to \boldsymbol{\sigma}. \tag{1.16}$$

So

$$\mathsf{H} \to \mathsf{H}' = \mp v \boldsymbol{\sigma} \cdot (\mathbf{k} + \mathbf{k}_0). \tag{1.17}$$

Therefore, if there is SIS, then there must be another nodal point at $-\mathbf{k}_0$ with opposite helicity.

When both TR and SI symmetries exist, each node would have two monopoles with opposite charges. The net topological charge of a nodal point (with 4 levels) is zero, and the Dirac node is not stable against perturbations (see Table I).

Note that when there is only SIS (but no TRS), then the minimum number of Weyl points in a solid is 2. If there is only TRS (but no SIS), then the minimum number is 4, since TRS-doublet would have a partner doublet with opposite helicity, as required by the Nielsen-Ninomiya theorem.

C. The Burkov-Balent multilayer model

Without diving into the subject of point group symmetry, here we introduce a simplified model proposed by Burkov and Balent (Burkov and Balents, 2011). Consider a structure with alternating layers of normal insulators

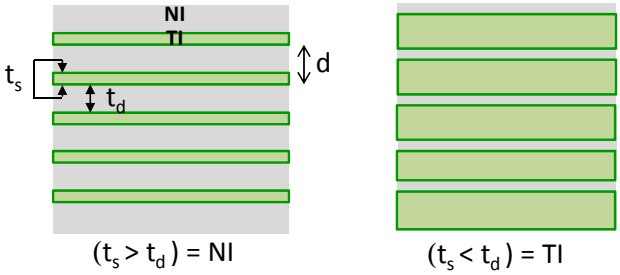

FIG. 4 A multi-layer structure with alternating layers of normal insulator (NI) and topological insulator (TI).

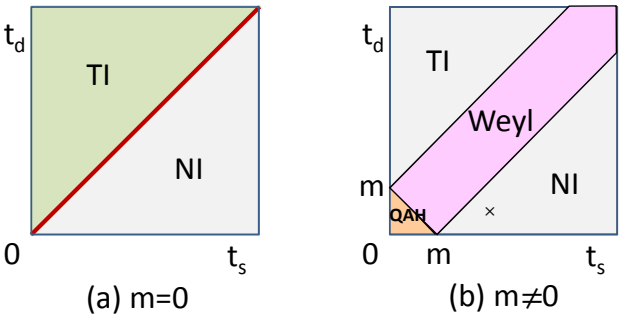

FIG. 5 (a) With both TRS and SIS, the critical line at $t_s = t_d$ are composed of unstable Dirac points. (b) After breaking the TRS with magnetization m, a Dirac point in (a) separates to two Weyl points and one has a finite region of Weyl semimetal phase. The gapped phase on the lower left is a quantum anomalous Hall phase. As m gets larger, the point $\times$ is first engulfed by the Weyl phase, then the QAH phase.

(NI) and topological insulators (TI) stacked along the z-axis (see Fig. 4). Coupling of the top and down surface states (SS) of a TI layer is written as t_s; coupling of SS between nearest-neighbor TI layers is written as t_d.

When the intra-layer coupling is larger than the inter-layer coupling ($t_s > t_d$), the whole structure is similar to a NI. On the other hand, when $t_d > t_s$, the whole structure is similar to a TI. By tuning the relative strength between t_s and t_d, one can induce a topological phase transition at certain critical value. At that value the bulk gap is expected to close, probably producing a point degeneracy.

However, from the analysis in previous section, we know that with both TRS and SIS, this degenerate (Dirac) point would be unstable. The degeneracy would be lifted when one slightly moves away from the critical value (see Fig. 5(a)). To stablize it, one can break the TRS, for example.

For one TI slab, the Hamiltonian with the SS coupling is,

$$\mathsf{H} = v\tau_z \otimes (\boldsymbol{\sigma} \times \mathbf{k}_\perp) \cdot \hat{z} + t_s \tau_x \otimes 1 + m 1 \otimes \sigma_z, \quad (1.18)$$

in which $\boldsymbol{\tau}$ accounts for the up and down layers degree of freedom, and m is the magnetization. From now on we will drop the $\otimes$ sign.

For multiple-layers, we have

$$\begin{aligned} \hat{\mathsf{H}} &= \sum_l \left[v\tau_z(\boldsymbol{\sigma} \times \mathbf{k}_\perp) \cdot \hat{z} + t_s \tau_x + m\sigma_z \right] c_l^\dagger c_l \\ &+ \sum_l t_d(\tau_+ c_l^\dagger c_{l+1} + \tau_- c_l^\dagger c_{l-1}), \end{aligned} \quad (1.19)$$

where $\tau_\pm = (\tau_x \pm i\tau_y)/2$, $c_l = (c_{lu}, c_{ld})^T$ is a 2-component operator such that $\tau_+ c_l^\dagger c_{l+1} = c_{lu}^\dagger c_{l+1d} \cdots$ etc.

Assume there are N (NI+TI)-layers with period d, and impose the periodic BC along z-axis. Using the Fourier transformation,

$$c_l^\dagger = \frac{1}{\sqrt{N}} \sum_{k_z} e^{ildk_z} c_{k_z}^\dagger. \quad (1.20)$$

one has,

$$\begin{aligned} \hat{\mathsf{H}} &= \sum_{k_z} \Big[v\tau_z(\boldsymbol{\sigma} \times \mathbf{k}_\perp) \cdot \hat{z} c_{k_z}^\dagger c_{k_z} \\ &+ m\sigma_z c_{k_z}^\dagger c_{k_z} \\ &+ t_s \tau_x c_{k_z}^\dagger c_{k_z} \\ &+ t_d(e^{-ik_z d}\tau_+ c_{k_z}^\dagger c_{k_z} + e^{ik_z d}\tau_- c_{k_z}^\dagger c_{k_z}) \Big] \quad (1.21) \\ &= \sum_{k_z} \begin{pmatrix} \mathsf{h}_0 + m\sigma_z & t_s + t_d e^{-ik_z d} \\ t_s + t_d e^{ik_z d} & -\mathsf{h}_0 + m\sigma_z \end{pmatrix} c_{k_z}^\dagger c_{k_z}, \\ &\equiv \sum_{k_z} \mathsf{H}_{k_z} c_{k_z}^\dagger c_{k_z}, \quad (1.22) \end{aligned}$$

where

$$\begin{aligned} \mathsf{H}_{k_z} &= \tau_z \mathsf{h}_0 + m\sigma_z \\ &+ t_s\tau_x + t_d(e^{-ik_z d}\tau_+ + e^{ik_z d}\tau_-), \end{aligned} \quad (1.23)$$

and $\mathsf{h}_0 = v(\boldsymbol{\sigma} \times \mathbf{k}_\perp) \cdot \hat{z}$. Each k_z-subspace is independent of each other.

Under the unitary transformation (Burkov *et al.*, 2011),

$$\mathsf{U} = \begin{pmatrix} 1 & 0 \\ 0 & \sigma_z \end{pmatrix} \quad (1.24)$$

one has

$$\tau_{x,y} \to \mathsf{U}^\dagger \tau_{x,y} \mathsf{U} = \tau_{x,y}\sigma_z, \quad (1.25)$$

$$\sigma_{x,y} \to \mathsf{U}^\dagger \sigma_{x,y} \mathsf{U} = \tau_z \sigma_{x,y}. \quad (1.26)$$

τ_z and σ_z are not changed.

After the transformation,

$$\begin{aligned} \mathsf{H}_{k_z} &= \mathsf{h}_0 + m\sigma_z \\ &+ [t_s\tau_x + t_d(e^{-ik_z d}\tau_+ + e^{ik_z d}\tau_-)]\sigma_z. \end{aligned} \quad (1.27)$$

One can rotate the $\boldsymbol{\tau}$ on the 2nd line without changing the first line. Thus, the Hamiltonian is decomposed to 2

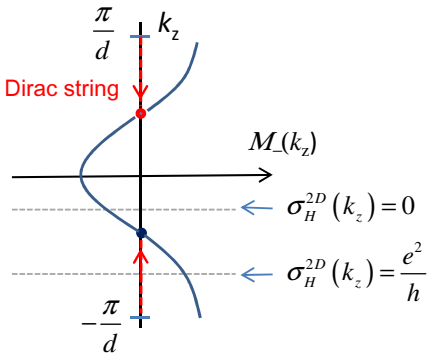

FIG. 6 $M_-(k_z)$ plotted as a function of k_z (rotated by 90 degrees).

diagonal blocks,

$$\mathsf{H}_{k_z} = \mathsf{h}_0 + \underbrace{\left[m + \tau_z\sqrt{t_s^2 + t_d^2 + 2t_s t_d\cos(k_z d)}\right]}_{M_{\tau_z}(k_z)}\sigma_z, \tag{1.28}$$

where $M_\pm(k_z)$ can be considered as the effective masses of the 2D electron gas in the k_z-layer.

Finally, the 2×2-blocks can be easily diagonalized to get the eigenvalues,

$$\varepsilon_\pm^{\tau_z} = \pm\sqrt{v^2(k_x^2+k_y^2) + M_{\tau_z}^2(k_z)}. \tag{1.29}$$

Let $m>0$, then $M_+(k_z)$ is always positive, and $\varepsilon_\pm^+$ has a finite gap. On the other hand, $\varepsilon_\pm^-$ can be gapless if $M_-(k_z)=0$, or

$$\cos(k_0 d) = \frac{m^2 - (t_s^2+t_d^2)}{2t_s t_d}. \tag{1.30}$$

That is, if

$$\underbrace{|t_s - t_d|}_{m_{c1}} \le m \le \underbrace{|t_s + t_d|}_{m_{c2}}, \tag{1.31}$$

then there are a pair of Weyl nodes at $\pm k_0\hat{z}$ (see Figs. 5(b) and 6).

If $m<|t_s-t_d|$, then Eq. (1.30) has no real solution, and $M_-(k_z)<0$. If $m>|t_s-t_d|$, then Eq. (1.30) has no real solution, and $M_-(k_z)>0$. For small m, the material is a trivial insulator. The pair of Weyl nodes appear at $k_z d=\pi$ when $m=m_{c1}$. They move apart along the k_z-axis when $m>m_{c1}$, and merge with each other again at $k_z=0$ when $m=m_{c2}$ (see Fig. 7). After that, the energy gap is re-opened, but the system becomes a non-trivial insulator (see below).

We now focus on the Weyl semi-metal phase. As shown in Eq. (1.22), the system is composed of decoupled 2D sub-systems, each has their own k_z-layer of 2D BZ . Since the Weyl point is a 3D monopole, it has a string of gauge singularity (Dirac string). The location of the string is gauge dependent, but they should connect the two Weyl

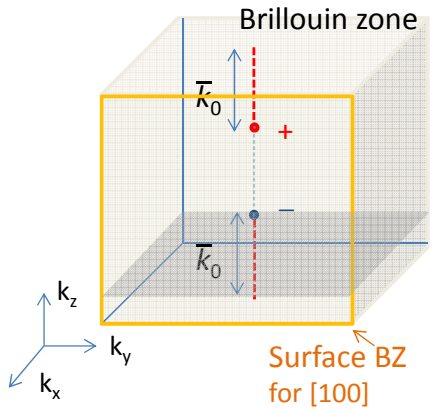

FIG. 7 A pair of Weyl points appear at $k_z=\pi$ when $m=m_{c1}$. They stretch out a Dirac string (red dotted lines) at larger m, and finally merge with each other at $m=m_{c2}$, but leaving a full Dirac string behind.

nodes (see Fig. 7). The 2D k_z-layers within $|k_z|<k_0$ ($M_-(k_z)<0$) do not intersect with the gauge singularity, and the first Chern number $C_1=0$. On the other hand, the k_z-layers outside of that range would intersect with the gauge singularity, and have a vortex in each of the 2D BZ. This leads to $C_1=1$, and $\sigma_H^{2D}(k_z)=e^2/h$ for each of the 2D-subsystem. See Sec **??** for the discussion of the vortex in the BZ of a quantum Hall system.

As a result, the 3D Hall conductivity is

$$\begin{aligned}\sigma_H^{3D} &= \frac{1}{L}\sum_{k_z}\sigma_H^{2D}(k_z)\\ &= \int_{-\pi/d}^{\pi/d}\frac{dk_z}{2\pi}\sigma_H^{2D}(k_z) = \frac{e^2}{h}\frac{\bar{k}_0}{\pi},\end{aligned} \tag{1.32}$$

where $\bar{k}_0=\pi/d-k_0$ is half the length of the Dirac string.

When $m=m_{c2}$, the two nodes merge at $k_z=0$, and the Dirac string spans the whole k_z-axis. After that, the system enters the semi-quantum anomalous Hall phase with

$$\sigma_H^{3D} = \frac{e^2}{h}\frac{1}{d}. \tag{1.33}$$

1. Fermi arc of surface states

Divide the space into two parts, with the magnetization

$$\begin{aligned} m(x) &< |t_s - t_d| \text{ for } x<0,\\ m(x) &> |t_s - t_d| \text{ for } x>0,\end{aligned} \tag{1.34}$$

and $m(x)$ increases monotonically from one side to the other. Ignoring the unfilled $M_+(k_z)$ block, the remaining two-state Hamiltonian for a 2D sub-system is (see

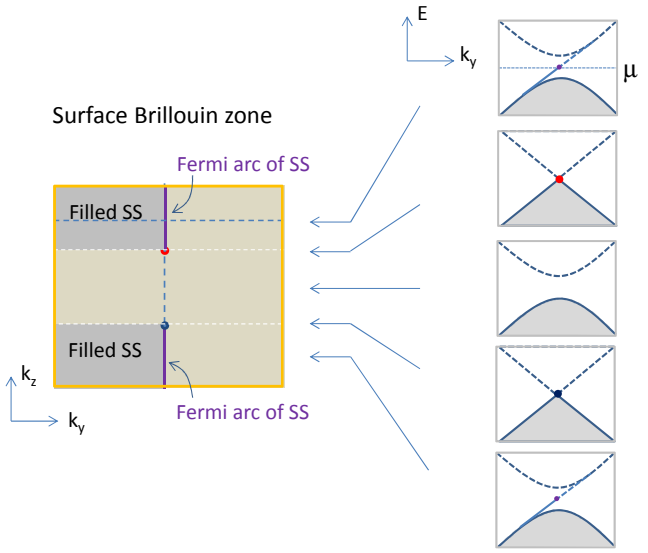

FIG. 8 Fermi arc of the SS in a 2D surface BZ. Five slices of the 1D edge BZ of the 2D k_z-subsystem are shown on the right.

Eq. (1.28))

$$\mathsf{H}_{k_z} = \mathsf{h}_0 + \underbrace{\left[m(x) - \sqrt{t_s^2 + t_d^2 + 2t_s t_d \cos(k_z d)}\right]}_{M_-^{k_z}(x)} \sigma_z. \tag{1.35}$$

Similar to the analysis of the edge states of the QWZ model in Chap. **??**, first replace k_x by the differential operator $\frac{1}{i}\frac{\partial}{\partial x}$. One then solves the following differential equation to find the edge state,

$$\begin{pmatrix} M_-^{k_z}(x) & v\left(\frac{\partial}{\partial x} + k_y\right) \\ v\left(-\frac{\partial}{\partial x} + k_y\right) & -M_-^{k_z}(x) \end{pmatrix} \phi_s^{k_z} = \varepsilon_s^{k_z}(k_y)\phi_s^{k_z}. \tag{1.36}$$

A trial solution that decays inside the Weyl semimetal at $x > 0$ is,

$$\phi_s^{k_z}(x) = e^{-\frac{1}{v}\int_0^x dx' M_-^{k_z}(x)} \begin{pmatrix} 1 \\ 1 \end{pmatrix}. \tag{1.37}$$

One can verify that it is indeed an eigenstate, with eigenvalue $\varepsilon_s^{k_z}(k_y) = vk_y$, which is linear in k_y and independent of k_z.

The energy dispersion of the surface states is a 2D surface in the 3D BZ. The surface BZ for the [100] surface is shown in Fig. 8, with 5 slices of the energy dispersion shown on the right. A 2D subsystem with $C_1 = 0$ is a trivial 2D insulator, which has no edge state. A 2D subsystem with $C_1 = 1$ is similar to a 2D quantum Hall system, which has chiral edge state. The electrons fill up to a Fermi point in its 1D edge BZ. By connecting these points from different k_z's, one sees that the SS electrons of the Weyl semimetal would fill up to a Fermi line (aka **Fermi arc**, Wan *et al.*, 2011). For more details, see Yang *et al.*, 2011 and Okugawa and Murakami, 2014. Also see Potter *et al.*, 2014 for an illuminating analysis of the SS and the Fermi arc. The relation between group symmetry and the effective Hamiltonian near a Weyl point can be found in Fang *et al.*, 2012.

Experimentally, transition metal monopnictides such as TaAs (Lv *et al.*, 2015; Xu *et al.*, 2015b), and NbAs (Xu *et al.*, 2015a) have been confirmed as Weyl semimetals, and their Fermi arcs observed.

Exercise

1. Instead of breaking TRS, one can break the SIS of the Burkov-Balent model, for example, by unbalancing the top-bottom layers of the TI slabs. That is, by adding a term $V_0\tau_z$ to the Hamiltonian ($t_{s,d} > 0$),

$$\begin{aligned} \mathsf{H} &= \tau_z \mathsf{h}_0 + V_0\tau_z \\ &+ t_s\tau_x + t_d(e^{-ik_z d}\tau_+ + e^{ik_z d}\tau_-), \end{aligned} \tag{1.38}$$

where $h_0 = v(\boldsymbol{\sigma} \times \mathbf{k}_\perp) \cdot \hat{z}$.
(a) Given the SI operator $\Pi = \tau_x$, show that the Hamiltonian with $V_0 = 0$ has SIS, $\Pi\mathsf{H}(\mathbf{k})\Pi^{-1} = \mathsf{H}(-\mathbf{k})$, while V_0 breaks it.
(b) Switch from the basis $\boldsymbol{\tau} \otimes \boldsymbol{\sigma}$ to the basis $\boldsymbol{\sigma} \otimes \boldsymbol{\tau}$, perform a rotation in $\boldsymbol{\tau}$-space to block-diagonalize the Hamiltonian, then find out the eigenvalues $\varepsilon_\pm^{\sigma_z}$ of H.
2. Following Prob. 1, (a) show that when $t_s = t_d$, the middle two bands touch at a circle of line degeneracy at $k_z = \pi/d$. Such a degeneracy requires the fine-tuning of t_s and t_d, and therefore is not robust.
(b) Break the rotational symmetry around k_z by having

$$t_{s,d} = t_{s,d}^0 + t'_{s,d}k_x^2 \tag{1.39}$$

$$= t_{s,d}^0 + t'_{s,d}k_\perp^2 \cos^2\theta. \tag{1.40}$$

Show that, when $t_s = t_d$, there are point degeneracies at

$$\cos 2\theta = \frac{2(t_s^0 - t_d^0)}{k_\perp^2(t'_d - t'_s)} - 1. \tag{1.41}$$

(c) The multilayer structure is a normal insulator when $t_s^0 > t_d^0$. Assume $t'_s > t'_d$, decrease the value of t_s^0 and investigate the creation and annihilation of Weyl points. (Ref: Halász and Balents, 2012)

References

Burkov, A. A., and L. Balents, 2011, Phys. Rev. Lett. **107**, 127205.

Burkov, A. A., M. D. Hook, and L. Balents, 2011, Phys. Rev. B **84**, 235126.

Chang, M.-C., and M.-F. Yang, 2015, Phys. Rev. B **92**, 205201.

Fang, C., M. J. Gilbert, X. Dai, and B. A. Bernevig, 2012, Phys. Rev. Lett. **108**, 266802.

Felsager, B., 1998, *Geometry, particles and fields* (Springer-Verlag, New York).

Halász, G. B., and L. Balents, 2012, Phys. Rev. B **85**, 035103.

Lv, B. Q., H. M. Weng, B. B. Fu, X. P. Wang, H. Miao, J. Ma, P. Richard, X. C. Huang, L. X. Zhao, G. F. Chen, Z. Fang, X. Dai, *et al.*, 2015, Phys. Rev. X **5**, 031013.

Milnor, J. W., 1965, *Topology from the differential viewpoint* (The University Press of Virginia, Charlottesiville).

Nielsen, H. B., and M. Ninomiya, 1981a, Nuclear Physics B **185**(1), 20.

Nielsen, H. B., and M. Ninomiya, 1981b, Nuclear Physics B **193**(1), 173.

Okugawa, R., and S. Murakami, 2014, Phys. Rev. B **89**, 235315.

Potter, A. C., I. Kimchi, and A. Vishwanath, 2014, Nature Communications **5**, 5161.

Wan, X., A. M. Turner, A. Vishwanath, and S. Y. Savrasov, 2011, Phys. Rev. B **83**, 205101.

Xu, S.-Y., N. Alidoust, I. Belopolski, Z. Yuan, G. Bian, T.-R. Chang, H. Zheng, V. N. Strocov, D. S. Sanchez, G. Chang, C. Zhang, D. Mou, *et al.*, 2015a, Nat Phys **11**(9), 748.

Xu, S.-Y., I. Belopolski, N. Alidoust, M. Neupane, G. Bian, C. Zhang, R. Sankar, G. Chang, Z. Yuan, C.-C. Lee, S.-M. Huang, H. Zheng, *et al.*, 2015b, Science **349**(6248), 613.

Yang, K.-Y., Y.-M. Lu, and Y. Ran, 2011, Phys. Rev. B **84**, 075129.